Comput. Methods Appl. Mech. Engrg. 200 (2011) 2256–2267

Contents lists available at ScienceDirect

Comput. Methods Appl. Mech. Engrg.

journal homepage: www.elsevier.com/locate/cma

Stochastic inverse identification of geometric imperfections in shell structures

Christopher J. Stull [a], Jonathan M. Nichols [b], Christopher J. Earls [c,*]

[a] Engineering Institute, Los Alamos National Lab., Los Alamos, NM 87545, USA
[b] Naval Research Laboratory, Optical Sciences Division, 4555 Overlook Ave. SW, Washington, DC 20375, USA
[c] Sch. of Civil and Env. Eng., Cornell University, 220 Hollister Hall, Ithaca, NY 14853, USA

ARTICLE INFO

Article history:
Received 22 November 2010
Received in revised form 10 March 2011
Accepted 21 March 2011
Available online 27 March 2011

Keywords:
Shell buckling
Initial imperfections
Stochastic inverse problems

ABSTRACT

It is now widely known that the presence of geometric imperfections in shell structures constitutes an important contribution to the discrepancy between theoretical and experimentally realizable ultimate loads governed by buckling. The present paper describes a method by which an actual initial imperfection field may be estimated using the service load response of a shell structure. The approach requires solving a stochastic inverse problem wherein uncertainty regarding initial imperfection predictions is expressed within the context of a Bayesian posterior distribution. The proposed approach could be applied to condition assessment and performance evaluation activities in practice.

1. Introduction

A recent and comprehensive survey of research developments during the period 1996 to 2006 [7] highlights the fact that understanding the nature and effects of imperfections in shell structures continues to be a fertile line of inquiry to this day. Since the publication of Koiter's seminal dissertation in 1945, it has become well known that initial geometric imperfections in shell structures may lead to dramatic erosions in ultimate strength [4,8,27]. However, the jump from this notional understanding, to the realization of a practically useful means for predicting the actual strength of in-service imperfect shell structures, is formidable. It is virtually impossible to rationally guess the precise imperfection field that may be manifest in a given structure; and thus it is problematic to know the buckling strength of this same structure.

The current research focuses on the *a posteriori* discovery of initial displacement imperfection fields (*i.e.* deviations from the archetypical geometry prior to any buckling) occurring due to manufacturing, fabrication, construction, or service conditions. While an earlier study in the literature [29] proposed an approach for the identification of initial imperfections in shell structures under service loading conditions, the earlier approach essentially embodied a *maximum likelihood estimate* (MLE) [12] in its identification of a single inverse solution representing the imperfection field. While MLEs possess many useful properties for estimation problems, they can present challenges when it comes to quantifying uncertainty in the parameter being estimated. The present research is, to the best of the authors' knowledge, a novel contribution in that uncertainty concerning this initial displacement estimate is quantified within the context of Bayes' Theorem, through the solution of a stochastic inverse problem effected using dependent sampling techniques [9,5,30].

1.1. Background

It is well known that experimentally observed buckling loads (or critical loads) for shell structures exhibit considerable scatter, when compared with theoretical predictions [4,26,27,7]. It is commonly assumed that the presence of initial displacement fields, causing deviations from the perfect shell geometry, are the primary cause of this scatter. Contributions from other sources of imperfection, related to boundary conditions, material properties, and shell thickness, are also important to consider [19–22]. However, given the pronounced effect that initial displacement fields have on the critical load (or buckling load) of shell structures [26,27], the present discussion will be restricted in scope to this type of shell structure imperfection. In this spirit, a detailed literature survey concerning the effects of imperfections in shell structures can be found in [29], and the references therein. However, it is important to mention two relatively more recent research efforts, as well as their relationship to the present work.

A recent study [25] focused on the influences of different sorts of imperfections within the context of steel I-shaped beam-columns. In this work, it was noticed that when considering the column-only response, the I-shaped members exhibited an interaction between the initial displacement and thickness imperfections that exceeded the influence of initial displacement effects alone (thickness-only influences were negligible). This would

* Corresponding author. Tel.: +1 607 255 1652.
E-mail address: earls@cornell.edu (C.J. Earls).

0045-7825/$ - see front matter © 2011 Elsevier B.V. All rights reserved.
doi:10.1016/j.cma.2011.03.012

support the notion that, in practice, the presence of thickness imperfections within the shell structure might also warrant consideration, but this is likely strongly dependent on the type of problem under consideration. Another recent study [13] explored an efficient optimization-based approach for obtaining a worst-case initial geometric imperfection field within a shell structure, as constrained by bounds on feasibility, as related to hypothetical deformations being explored by the optimization algorithm. These two recent studies focus on techniques that might lead to more principled design approaches. The present work seeks a more robust understanding concerning what is already there (*e.g.* within the context of a performance evaluation, *etc.*), and thus appears to be a novel contribution in that uncertainty concerning uncovered initial displacement imperfection predictions are quantified in a principled manner.

The present work is concerned with the development of a method that employs sparse sensor telemetry, acquired during a safe service loading condition, for use in the solution of a stochastic inverse problem that characterizes the actual, and previously unknown, displacement imperfection field in a shell structure. The initial displacement imperfection is assumed to be of a type consistent with denting (*i.e.* the imperfection field to be identified possesses a local length scale that is somewhat smaller than the overall shell structure dimensions). Once this *a posteriori* determination of the shell initial imperfection field is made, it is then used to make strength predictions regarding the shell structure in question. The method utilizes geometrically nonlinear finite element forward models, in conjunction with dependent sampling techniques, applied to a Bayesian posterior, in order to solve the system identification inverse problem related to the initial imperfection field.

1.2. Paper organization

A discussion of issues concerning the forward and inverse problem formulations related to the current research is given in Section 2 of the current paper; while Section 3 discusses salient features regarding the solution of a particular forward and inverse problem associated with edge supported barrel vault shells. Section 4 presents results from the inverse solutions, and provides context in the form of a discussion, in order that conclusions may be drawn in Section 5.

2. Problem formulation

As it is that shell buckling response in dented structures is ultimately at issue in this work, we require: a high-fidelity means for simulating shell structure performance in the perfect, and dented conditions; as well as the ability to propose hypothetical simulation cases for comparison with some noisy, sparse measurements from an actual shell structure. In this spirit, the present discussion concerning our problem formulation maintains generality; delaying details regarding implementation to later sections, within the sequel.

2.1. General forward problem formulation

In the most general context, the current problem is formulated on a domain $\overline{\Omega} = \Omega \cup \partial\Omega, \overline{\Omega} \subset \mathbb{R}^3$, with boundary, $\partial\Omega$, separated into regions of Dirichlet constraints, $\partial\Omega_E$, and regions of prescribed Neumann conditions, $\partial\Omega_N$, such that $\partial\Omega = \partial\Omega_E \cup \partial\Omega_N$ and $\partial\Omega_E \cap \partial\Omega_N = \emptyset$. On this problem domain, we may state a requirement for statical equilibrium within the context of elastic material response

$$\nabla \cdot \bar{\sigma} = 0, \quad \bar{\sigma} = \overline{C}^{IV} : \bar{\epsilon}(u(\vec{x})), \quad \forall \vec{x} \in \Omega \subset \mathbb{R}^3, \tag{1}$$

where $u(\vec{x})$ is the displacement field satisfying all Dirichlet boundary conditions, and $\overline{C}^{IV}$ is the fourth order tensor relating Green–Lagrange strain, $\bar{\epsilon}$, and the work conjugate Second Piola–Kirchhoff stress, $\bar{\sigma}$.

In preparation for an implementation involving the nonlinear finite element approach, the foregoing strong form is converted to a *weak form* by way of Galerkin projection [23], along with a subsequent weakening of continuity requirements through an application of Green's Lemma [14]; resulting in the following equality between a bilinear form and linear functional as:

$$a(\mathcal{U}, \mathcal{V}) = \langle \ell, \mathcal{V} \rangle, \tag{2}$$

where $\mathcal{U}$ are the *trial functions* and $\mathcal{V}$ are the *test functions* that "live" in spaces with the following properties:

$$\mathcal{U} \in H^{\alpha}_{\psi}(\Omega) = \{u : D^{\alpha}u \in L^2(\Omega), \quad \forall \alpha \in \mathbb{Z}^+ \ni \alpha \leqslant 1 \quad \text{and} \quad u = \psi \quad \text{on} \quad \partial\Omega\}, \tag{3}$$

$$\mathcal{V} \in H^{\alpha}_{o}(\Omega) = \{v : D^{\alpha}u \in L^2(\Omega), \quad \forall \alpha \in \mathbb{Z}^+ \ni \alpha \leqslant 1 \quad \text{and} \quad v = 0 \quad \text{on} \quad \partial\Omega\}, \tag{4}$$

where D^{α} are the *distributional derivatives* of order α and below. It is pointed out that all such boundaries are Lipschitz, and the essential conditions, ψ, are enforced in the sense of traces [23]. Ultimately, nonlinear shell finite elements will be used to effect a solution of the shell buckling problem considered herein. Details concerning the implementation will appear in the sequel.

2.2. General stochastic inverse problem formulation

In the present work, we assume a statically configured sensor array that acquires N temporally ordered samples from the K sensors, sparsely deployed on a shell structure. We will assume a linearly additive noise model for our sensor outputs, of the form [28]:

$$u^{exp}_{i,j} = u^{FEA}_{i,j}(\vec{\theta}) + \eta_{i,j}, \tag{5}$$

where $u^{exp}_{i,j}$ is some sparsely measured response of the real shell structure, and $u^{FEA}_{i,j}$ is some assumed suitable deterministically modeled response at sensor location i and time position j, as instantiated by the collection of P physical model parameters $\vec{\theta} = (\theta_1, \ldots, \theta_P)$ (*i.e.* corresponding to some initial displacement instance). It is pointed out that the discrete time index is related to continuous time via the sampling interval associated with the data collection. The job of the estimator is: given the data $u^{exp}_{i,j}$, produce values of the parameter vector $\vec{\theta}$ that generate good model predictions. Therefore, most estimation approaches proceed by forming an expression for the likelihood that a model, with a given $\vec{\theta}$, produces the observed data.

It will be assumed that the noise at the spatio-temporal points i, j are *i.i.d.* and drawn from a stationary, zero-mean, normal *probability distribution function* (PDF) of (unknown) variance σ^2; *i.e.* each noise value is distributed according to

$$p_{\eta}(\eta_{i,j}) = \frac{1}{\sqrt{2\pi\sigma^2}}\, e^{-\frac{1}{2\sigma^2}\eta^2_{i,j}}. \tag{6}$$

In our notation $p_a(b)$, for example, denotes the PDF $p_a()$ associated with random variable b. From Eq. (5) we recognize that:

$$\eta_{i,j} = u^{exp}_{i,j} - u^{FEA}_{i,j}(\vec{\theta}), \tag{7}$$

whereupon we may further observe the noise probability distribution to be:

$$p_{\eta}(\eta_{i,j}) = p_{\eta}\left(u^{exp}_{i,j} - u^{FEA}_{i,j}(\vec{\theta})\right), \tag{8}$$

which immediately implies the form of the *likelihood* [12] as:

$$p_\eta\left(u_{i,j}^{exp}\middle|u_{i,j}^{FEA}(\vec{\theta})\right) = \frac{1}{\sqrt{2\pi\sigma^2}}\; e^{-\frac{1}{2\sigma^2}\left(u_{i,j}^{exp}-u_{i,j}^{FEA}(\vec{\theta})\right)^2}. \tag{9}$$

We may now exploit the stationary and *i.i.d.* assumptions on our noise, to construct the likelihood for the jointly distributed multi-dimensional case, taken over $[1,K]\times[1,N]$ spatio-temporal points, as the products of the marginal distributions:

$$\begin{aligned} p_\eta\left(u_{i,j}^{exp}\middle|u_{i,j}^{FEA}(\vec{\theta})\right) &= \prod_i^K\prod_j^N \frac{1}{\sqrt{2\pi\sigma^2}}\; e^{-\frac{1}{2\sigma^2}\left(u_{i,j}^{exp}-u_{i,j}^{FEA}(\vec{\theta})\right)^2} \\ &= \frac{1}{\left(2\pi\sigma^2\right)^{\frac{K\times N}{2}}}\; e^{-\frac{1}{2\sigma^2}\sum_i^K\sum_j^N\left(u_{i,j}^{exp}-u_{i,j}^{FEA}(\vec{\theta})\right)^2} \\ &\equiv p_\eta(\vec{u}^{exp}|\vec{\theta}). \end{aligned} \tag{10}$$

It is pointed out that the likelihood function describes the probability of having observed a specific sequence of values $u_{i,j}^{exp}$. A reasonable, and popular, approach to estimation is to find the parameters that maximize this function: producing so-called *maximum likelihood estimates*. Uncertainty in such estimates is usually captured by repeating the estimation procedure a large number of times, and quantifying uncertainty in the result. Alternatively, one can make certain assumptions about the estimator, and number of data, in which case bounds on the estimator variance may be obtained. However, we are often more interested in the uncertainty in the quantity being estimated, as opposed to the estimator.

An alternative approach to estimation is to treat the unknown parameters as random variables and estimate their governing probability density functions. Such an approach is made possible by application of Bayes' Theorem, which relates the desired parameter distribution to the likelihood via:

$$p_{\vec{\theta}}\left(\vec{\theta}|\vec{u}^{exp}\right) = C^{-1}p_\eta\left(\vec{u}^{exp}|\vec{\theta}\right)p_\pi(\vec{\theta}), \tag{11}$$

wherein $p_\pi(\vec{\theta})$ is the so-called *prior* (embodying any prior understanding concerning the parameter set $\vec{\theta}$), and $p_{\vec{\theta}}(\vec{\theta}|\vec{u}^{exp})$ is the joint parameter *posterior* distribution. The normalizing constant C is given by the multi-dimensional integral $\int_{\mathbb{R}^P} p_\eta(\vec{u}^{exp}|\vec{\theta})p_\pi(\vec{\theta})d\vec{\theta}$. While Eq. (11) provides the joint (PDF), we are typically interested in the *marginal* distribution associated with the individual parameters (*e.g.* $p_{\theta_1}(\theta_1)$). Analytically this requires integrating Eq. (11) over each of the other parameters in the vector. Denoting the parameter vector with the ith parameter removed as $\vec{\theta}_{-i}$, the marginal distributions are found by

$$p(\theta_i) = \int_{\mathbb{R}^{P-1}} p\left(\vec{\theta}|\vec{u}^{exp}\right)d\vec{\theta}_{-i}. \tag{12}$$

Either the posterior mean, or the median, are commonly employed choices for the final parameter estimate. Additionally, we may use the posterior to form a credible interval for each parameter (*i.e.* the probability that the parameter falls in a specific interval). This is precisely the information that we are interested in. It will be shown in Section 3.2.1 how to numerically obtain the parameter posteriors without having to analytically solve Eq. (12).

3. Shell modeling with imperfections

The discussion now turns to describing the approaches taken in the forward solution of a specific shell buckling problem. The model problem geometry considered in the current work is displayed in Fig. 1. This problem is the basis for all results presented in the sequel. The selection of a portion of a cylindrical shell (barrel vault), with the associated pinned boundaries, is made in order to enhance imperfection sensitivity [7]. The present research intends to enable a means for inferring the presence of an initial imperfection field within the shell domain, to characterize it in a quantifiable way using service loading response, and then to make prognoses regarding the overall shell buckling strength. In light of these aims, it is important to address the type of imperfections being considered in this work.

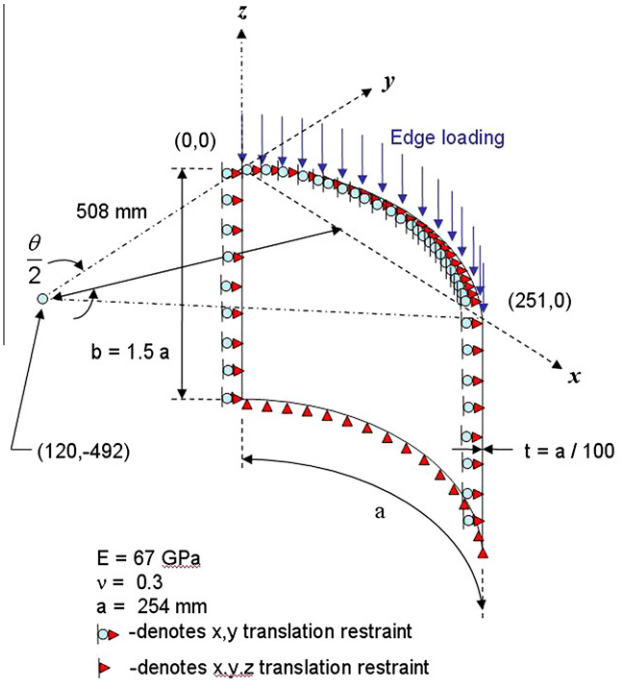

Fig. 1. Edge loaded barrel vault shell example structure.

A natural approach for modeling displacement imperfections that are consistent with denting (the focus of the present study) is to use Gaussian Radial Basis Functions (RBFs) [10]. The use of RBFs allows for a convenient parameterization of the initial imperfection field; subsequently facilitating the use of dependent sampling approaches for the solution of the stochastic inverse problem. The parameterization of the initial imperfection field adopted in the current work is given as:

$$u_o(\vec{x};\vec{\theta}) \approx \sum_{i=1}^{N}\{\omega\}_i\Psi_i(\vec{x}), \tag{13}$$

where

$$\Psi_i(\vec{x}) = e^{-\left(\frac{\|\tilde{c}_i-\vec{x}\|_{\ell 2}}{\sqrt{2}\tilde{\sigma}_i}\right)^2} \tag{14}$$

is a Gaussian RBF in which $\tilde{c}_i$ represent the radial basis centers and $\tilde{\sigma}_i$ are their standard deviations, and ω_i are the Fourier coefficients of the initial imperfection approximation [23]. In this work an ω_i of unity corresponds to an RBF with a height of 25.4 mm, for the model problem described in Fig. 1. A depiction of a single Gaussian RBF, superimposed on the model shell problem, is displayed in Fig. 2. Within the model problems, each particular dent will either be identified using a single RBF, or through a linear combination of four RBFs.

The $\tilde{c}_i$, $\{\omega\}_i$, and $\tilde{\sigma}_i$ variables will be treated as the primary unknowns in the inverse problem (*i.e.* it will be their distributions that are studied with respect to a dependent search of the Bayesian posterior). Thus, for "N" RBFs we may construct the unknown parameter vector consisting of $P = 3N + 1$ entries

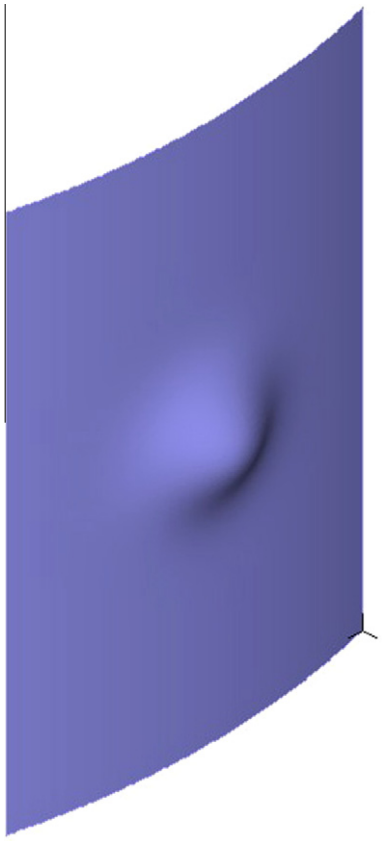

Fig. 2. Representative dent imperfection (magnified 1000x).

$$\vec{\theta} = \begin{Bmatrix} \tilde{c}_1 \\ \{\omega\}_1 \\ \tilde{\sigma}_1 \\ \vdots \\ \tilde{c}_N \\ \{\omega\}_N \\ \tilde{\sigma}_N \\ \sigma^2 \end{Bmatrix}, \tag{15}$$

where we have also included the noise variance term σ^2 in the unknowns. It is possible that one may know this parameter *a priori* and not need to solve for it, however as will be shown, adding the noise variance as a parameter incurs little computational cost.

3.1. Forward modeling

The forward modeling of the shell structure depicted in Fig. 1 is carried out within the context of the nonlinear finite element method (geometric nonlinearity only). Specifically, the four-node, assumed strain, shell finite element given by Bathe and co-workers (*i.e.* MITC4 Shell) [6,2,3] is employed in conjunction with the classical Newton–Raphson solution approach [14]. A detailed mesh convergence study carried out for collapse of the model problem (see Fig. 3 for a summary of these results) reveals that a MITC4 mesh with approximately 200,000 degrees of freedom represents an accurate mesh; suitable for use as the *ground truth* case within the context of the current inverse problem solution. A less dense mesh (having approximately 50,000 degrees of freedom) is thought to represent a reasonable compromise between modeling accuracy and computational expedience; thus this mesh is used in conjunction with the stochastic search algorithm (as the model employed in evaluating the likelihood function). The large number of analyses that are required for the solution of this type of inverse problem (*i.e.* potentially thousands of runs of the forward model) justifies the tradeoff in accuracy for solution speed. It is pointed out that while the standard Newton–Raphson nonlinear solution algorithm is used in the solution of the inverse problems, a hybrid solution algorithm, combining a modified spherical arc length method and the constant increment of external work method [1], is used in the collapse analyses associated with the mesh convergence study. It is further noted that imperfect meshes were used in the above mentioned convergence study, as per [21]. An approximation to the first global buckling mode, as obtained from a linearized eigenvalue buckling analysis, was employed as a means for perturbing the mesh geometry used during the nonlinear collapse analyses.

3.2. Inverse solution

3.2.1. Markov chain Monte Carlo sampling

Evaluating Eq. (11) for the marginal posterior distributions does not typically lend itself to analytical treatment; particularly if the parameter vector $\vec{\theta}$ is multi-dimensional (necessitating a multi-dimensional integral). Fortunately there exists a class of numerical approaches referred to as Markov Chain Monte Carlo (MCMC) methods. These approaches were first explored by Metropolis et al. [16] for solving high-dimensional integrals, and subsequently became well known in Bayesian estimation problems via the work of Hastings [11]. The MCMC method seeks to numerically generate K samples from the posterior distribution of interest, *i.e.* draw

$$\theta_i(k) \sim p_{\theta_i}(\theta_i) \;\; k = 1 \ldots K. \tag{16}$$

Hastings showed that this could be easily accomplished by creating a first order Markov chain $f(\theta_i(k+1)|\theta_i(k))$ provided that the distribution $f(\cdot|\cdot)$ obeyed certain properties [11]. Specifically, he showed that given a starting value $\theta_i(0)$, subsequent values could be generated by choosing a candidate value

$$\theta_i^* \sim q\left(\theta_i^* | \theta_i(k)\right) \tag{17}$$

via the candidate generating distribution function $q(\cdot)$, and subsequently evaluating the ratio

$$r = \frac{p_{\theta_i}(\theta_i^*) q(\theta_i(k)|\theta_i^*)}{p_{\theta_i}(\theta_i(k)) q(\theta_i^*|\theta_i(k))} = \frac{p_\eta(\vec{u}^{exp}|\theta_i^*) p_{\pi_i}(\theta_i^*)}{p_\eta(\vec{u}^{exp}|\theta_i) p_{\pi_i}(\theta_i)} \frac{q(\theta_i(k)|\theta_i^*)}{q(\theta_i^*|\theta_i(k))}. \tag{18}$$

The candidate value θ_i^* is accepted with probability min $(r,1)$ as $\theta_i(k+1) = \theta_i^*$, otherwise we retain the previous value $\theta_i(k+1) = \theta_i(k)$. The stationary Markov chain that results contains samples from the desired posterior distribution. Typically, however, there is a non-stationary transient period during the start of the chain, as the values converge toward their stationary distribution. Particularly, if the prior $\theta_i(0) \sim p_{\pi_i}(\theta)$ is poor, it may take some number of "burn-in" samples, B, before the influence of the data (influence of the likelihood in evaluating r) overwhelms the bad initial guess (*i.e.* "you can twist perception, reality won't budge" [24]). Provided that there are enough data, even a poorly chosen prior will often not significantly impact the result. The process repeats for $K > B$ samples, and the final $K - B$ values are taken to be truly representative samples from $p(\theta_i)$. For the univariate parameter vector, this completes the algorithm. However, one often deals with multi variate parameter vectors (as in the present case). This requires only a slight modification to the algorithm. The sampler is simply adjusted so that each parameter is taken in turn, holding the others fixed. In other words, for iteration k in the Markov chain, for the i^{th} parameter, we are sampling from the conditional posterior

$$p(\theta_i(k+1)|\theta_1(k+1), \ldots, \theta_{i-1}(k+1), \theta_{i+1}(k), \ldots, \theta_P(k)). \tag{19}$$

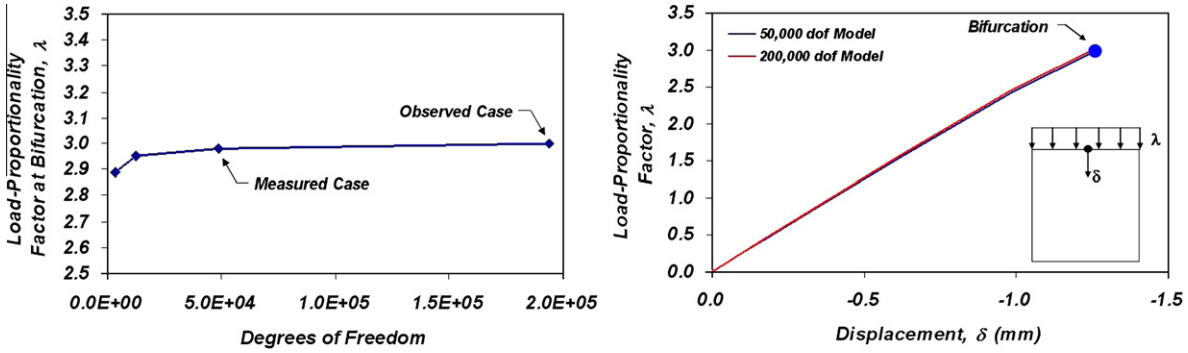

Fig. 3. Agreement in buckling predictions for meshes employed in likelihood evaluations (measured case) and as the simulated ground truth (observed case).

Each of the parameters are taken in turn, until we have sampled the entire vector $\vec{\theta}(k+1)$, at which point we increment k and begin the next iteration.

The requirements on the candidate generating distribution, $q(\cdot)$, are mild. It is only required that the distribution allow the parameter value to reach any other parameter value in a finite number of iterations. However, in practice some distributions afford faster convergence than others (*i.e.* less burn-in, and higher acceptance rates). In the current work a distribution of the following form is chosen:

$$q(\theta_i^*|\theta_i(k)) = \frac{1}{2A}, \quad |\theta_i^* - \theta_i(k)| < A, \tag{20}$$

i.e. the Uniform distribution with width A. Clearly this distribution is symmetric in exchange of its arguments, so that the ratio of candidate generating distributions in Eq. (18) cancel out, and r simply becomes the ratio of posterior distributions, evaluated at both the candidate and original values of the parameter. One can think of the proposal as applying a perturbation to the existing solution, and subsequent acceptance or rejection of that perturbation is dictated via the ratio r. The question of how to choose the *size* of the perturbation, A in this case, has received much attention in the literature [17,18]. Too large a perturbation and parameter values are unlikely to be accepted; too small and it will take prohibitively long times to explore the parameter space. Here, a simple "tuning" strategy is adopted; whereby A is modified during the burn-in period such that a target probability of acceptance is achieved. Following the approach outlined in [15], A is multiplied by a small constant α after acceptance, or divided by a constant, if the sample is rejected. This tuning is gradually phased out during the course of the burn-in period. Thus, after acceptance

$$A = A \times \left(\alpha - (\alpha - 1)\frac{k}{B}\right) \tag{21}$$

is applied, and after rejection

$$A = A \Big/ \left(\frac{1 - p_{accept}}{1 - p_{accept}\left(\alpha - (\alpha - 1)\frac{k}{B}\right)}\right) \tag{22}$$

is applied. In this work, $\alpha = 1.01$ and $p_{accept} = 0.42$, as recommended in [15].

While the MCMC approach is required for dependent sampling over the support of the posterior, in order that a histogram might be constructed, an alternate approach may be adopted for the noise variance.

3.2.2. Noise variance sampling

It turns out that if we can formulate a parameter prior that is conjugate to the likelihood, a direct sampling of the parameter posterior is possible (*i.e.* the form of the posterior will be known), without having to resort to the costly Metropolis–Hastings procedure outlined in the previous section. It is known that the conjugate prior for use in estimating the *precision*, $\lambda = \frac{1}{\sigma^2}$, of a *Gaussian* likelihood is the *Gamma* distribution, $\Gamma(\cdot)$ [5]. If one multiplies a Gamma distribution by a multivariate Gaussian (our likelihood) and applies the normalizing constant in Eq. (11), the posterior precision distribution is found to be:

$$p_\lambda(\lambda|\vec{\theta}, \vec{u}^{exp}) = \lambda^{\alpha'-1} e^{-\beta'\lambda} \frac{\beta^{\alpha'}}{\Gamma(\alpha')}, \tag{23}$$

where $\alpha' = \alpha + \frac{(K+N)}{2}$ and $\beta' = \beta + Q(\vec{u}^{exp}, \vec{\theta})$; with $Q(\vec{u}^{exp}, \vec{\theta})$ being the *Mahalanobis norm* defined as:

$$Q(\vec{u}^{exp}, \vec{\theta}) = \sum_i^K \sum_j^N \left(u_{i,j}^{exp} - u_{i,j}^{FEA}(\vec{\theta})\right)^2. \tag{24}$$

As part of the present work, Gamma distribution parameters are selected to ensure a diffuse prior and so $\alpha = 1$ and $\beta = 0$, thus yielding a distribution that enables an estimation of the noise variance:

$$\sigma^2 \sim \frac{1}{\Gamma\left(\frac{(K+N)}{2} + 1, \frac{2}{Q(\vec{u}^{exp}, \vec{\theta})}\right)}. \tag{25}$$

It is this distribution that is sampled from during each likelihood evaluation, occurring during the MCMC procedure, thus leading to a quantification of uncertainty regarding the noise variance in the system.

4. Results and discussion

As a means for investigating the behavior of the proposed approach for *a posteriori* imperfection identification in shell structures, a series of four test problem contexts are considered. Since a single problem geometry (Fig. 1) is shared by the four problem contexts, the difference comes in how the representation of single, centrally positioned denting imperfection (Fig. 4) is described during *a posteriori* identification. All problem contexts considered comprise an effort to solve a stochastic inverse problem, so as to identify the "ground truth" denting imperfection (*i.e.* the actual dent present in the "field".) The solution of the stochastic inverse problem is effected through a dependent search over the support of the relevant Bayesian posterior associated with each of the four contexts considered, as discussed in earlier sections of the present paper.

The results presented in the current section will begin with a discussion that focuses on the representation of the denting imperfection via a single RBF (*i.e.* the parameter set defining the Bayesian posterior in this case is five.) Additional results will then follow for the case where a linear combination of four RBFs are employed (*i.e.* the parameter set defining the Bayesian posterior in this case is seventeen.) This latter case is more realistic, since it is difficult to

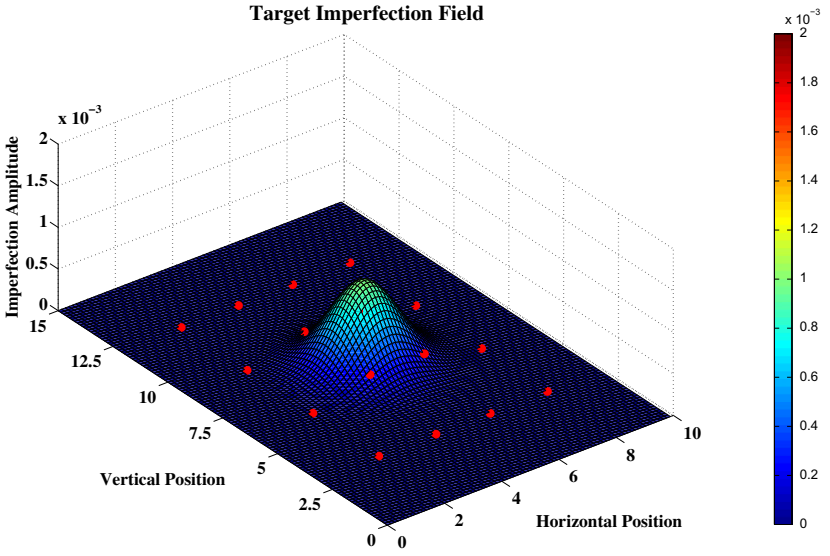

Fig. 4. Target imperfection field (magnified ≈ 2700x) with red dots denoting the sixteen sensor locations. (For interpretation of the references to colour in this figure legend, the reader is referred to the web version of this article.)

know, *a priori*, the number of dents that may be present in a hypothetical ground truth, and so the consideration of some number of RBFs is likely needed in any practical implementation.

In all of the present modeling contexts, the *ground truth* condition is generated using the converged shell finite element mesh described earlier (≈ 200,000 dof case). The edge loading is limited to be at a condition consistent with some hypothetical *service condition* (arbitrarily selected to be approximately 70% of the critical buckling load computed in the mesh convergence portion of the present work.) In this way, the present approach is seen as a way to use the response of the shell structure, at service loading, in order to identify the initial imperfection field that must be present within the structure.

As it is that a finite element model is used to generate surrogate experimental data, two different approaches are adopted for all results presented herein. Noise free and noise-contaminated cases are alternately applied as the ground truth measurements in the cases where either a single RBF, or four RBFs are used to describe the denting imperfection. It is pointed out that the noise free single RBF case does not constitute an *inverse crime* situation, as the ground truth model possesses a significantly different mesh density, as compared with the model used in evaluating the likelihood function. This additional source of modeling error will show up as additional "noise" in the modeling results, as described later in this section. Besides the effects of differences in mesh density between the ground truth and likelihood model instances, injected noise contamination is considered for one and four RBF contexts; wherein noise (see Eq. (5)) contamination of the ground truth is effected by adding, to the finite element model response, samples from a zero-mean Gaussian PDF, $\mathcal{N}(0, \sigma^2_{\text{SNR}})$, where

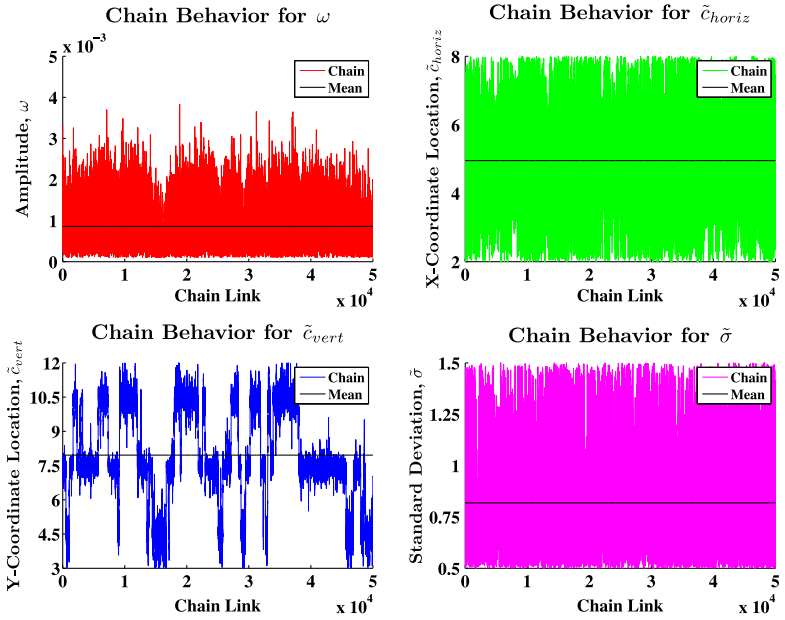

Fig. 5. One RBF: Markov chain behaviors of posterior parameters for noise free case: upper-left - amplitude; upper-right - horizontal location; lower-left - vertical location; lower-right - standard deviation.

$$\sigma_{\text{SNR}} = \frac{\frac{1}{n}\sum_{i=1}^{n} u_{ij}^{exp}}{\text{SNR}}. \tag{26}$$

Here, n is equal to the number of data sampling points employed in the inference problem (for the present case, $n = 16$, as identified from an earlier sensitivity study [29]) and SNR is the imposed signal-to-noise ratio of 1000. In the interest of brevity, noise free and noise-contaminated cases are discussed for the one RBF context, whereas only the noise-contaminated case is discussed for the four RBF context (since the four RBF noise free behavior is consistent with that observed in the solution of the one RBF noise free case). To summarize: the noise free case possesses some "noise" due to the difference in mesh density applied to the ground truth and likelihood model instances (*i.e.* there is a non-negligible, and different, projection error in going from the continuous solution space to each of the two discrete finite element sub-spaces associated with the two distinct meshes), while the noise-contaminated cases include this discretization error *in addition to* the injection of randomly sampled Gaussian noise. Thus, it is noted that all results presented (*i.e.* "noise free" and "noise-contaminated" cases) contain a projection error, but the latter case possesses *additional* noise, injected using a Gaussian PDF.

For each of the problem contexts discussed below, following burn-in (see Section 3.2.1), 50,000 Markov chain links are completed. It is noted that the computational effort expended in the present work is significantly greater than that of most MLE methods. However, the MLE methods fail to furnish insight into the uncertainty accompanying their prediction regarding the nature of the imperfection field identified. The MLE methods yield a parameter set defining the imperfection field identified [29], whereas the current approach uncovers a posterior probability density function that enables a quantification of the uncertainty concerning these parameters, as they pertain to predictions concerning the actual imperfection field present on the given shell structure.

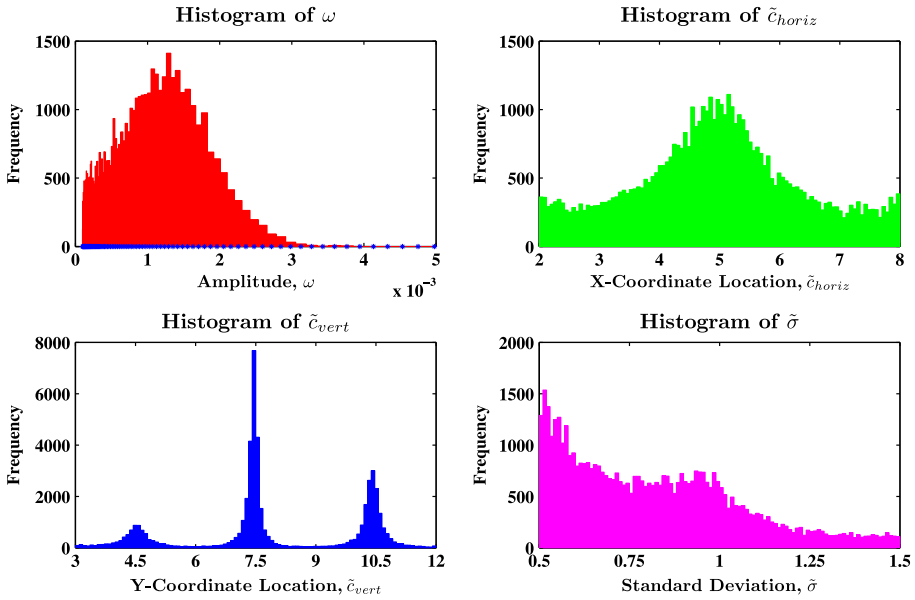

Fig. 6. One RBF: histograms of posterior parameters for noise free case (locations as in Fig. 5).

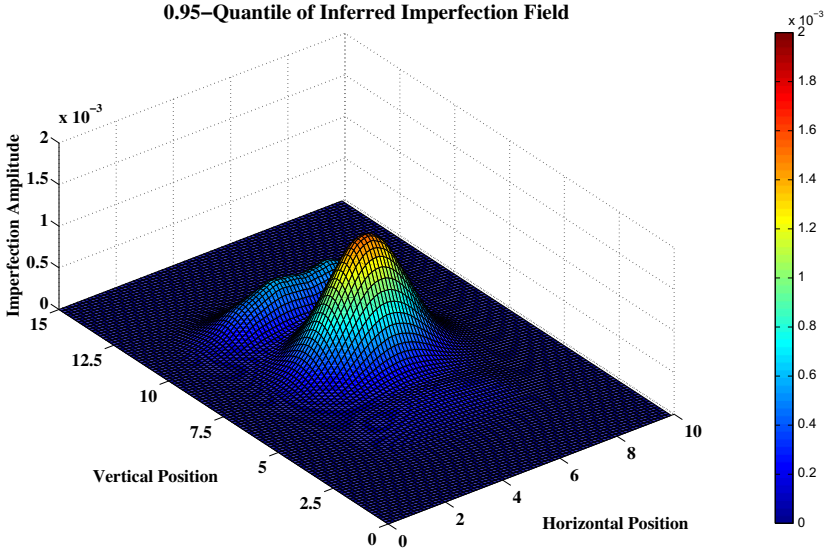

Fig. 7. One RBF: 95% Quantile of denting imperfection for noise free case (magnified ≈ 2700x).

4.1. 1 RBF contexts

4.1.1. Noise free results

Fig. 5 illustrates the chain behaviors for each of the four parameters defining the Bayesian posterior for this context. In the case of the dent location, it is noticed that the support of the distribution respects the physical dimensions of the shell domain (*i.e.* a uniform prior is employed over the shell geometric dimensions). As seen in the lower-left plot, the MCMC inference process identifies three distinct vertical locations in which the imperfection may plausibly occur. However, a more thorough examination of these chains reveals further information about the detection problem, which was not made available by the MLE exercise given in [29]. Considering the amplitude (upper-left) and vertical location (lower-left) chain behaviors, it can be seen that lower-amplitude imperfections favor vertical locations nearer to the bottom of the shell structure. Additionally, there is a relation between the dent extent (*i.e.* RBF standard deviation (lower-right)) and the vertical location, in which "tighter" imperfections favor vertical locations nearer to the top of the structure. It is noted that the noise-contaminated case presented in the sequel, yields similar results; a corresponding figure is omitted for brevity.

Fig. 6 provides scaled PDFs of the four model parameters, emanating from the inference process. As in the qualitative analysis of Fig. 5, a clear preference toward three distinct vertical locations is also observed in Fig. 6. It is noted that in [29], the authors mentioned this as a possible reason why the optimization algorithm (*i.e.* a genetic algorithm) may have become "trapped" in a suboptimal location, but no *quantitative* evidence could be furnished in this earlier study. This is precisely where inference methods excel (at the expense of additional forward runs), in that quantitative evidence is provided which can be employed to substantiate these earlier claims.

While the individual Markov chains and PDFs are helpful in developing a better understanding of the problem at hand, Fig. 7 provides a more convenient means of visualizing these results;

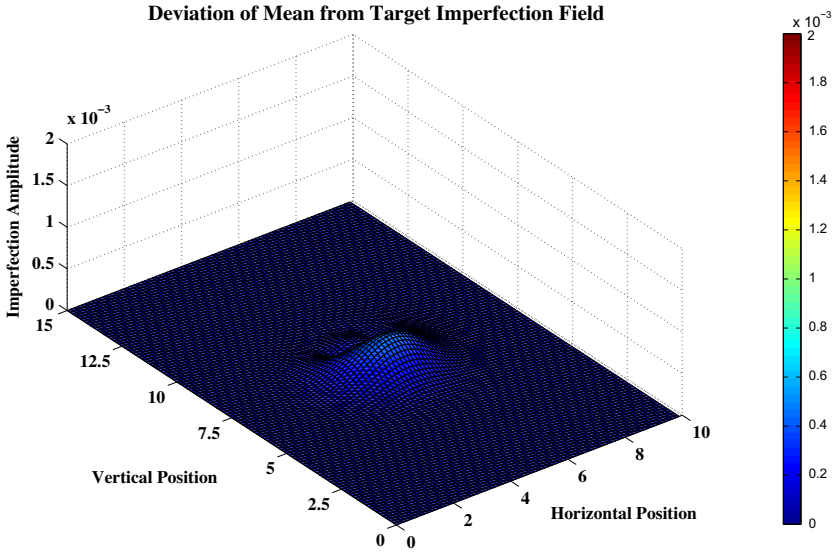

Fig. 8. One RBF: deviation of mean from the target imperfection field for noise free case (magnified ≈ 2700x).

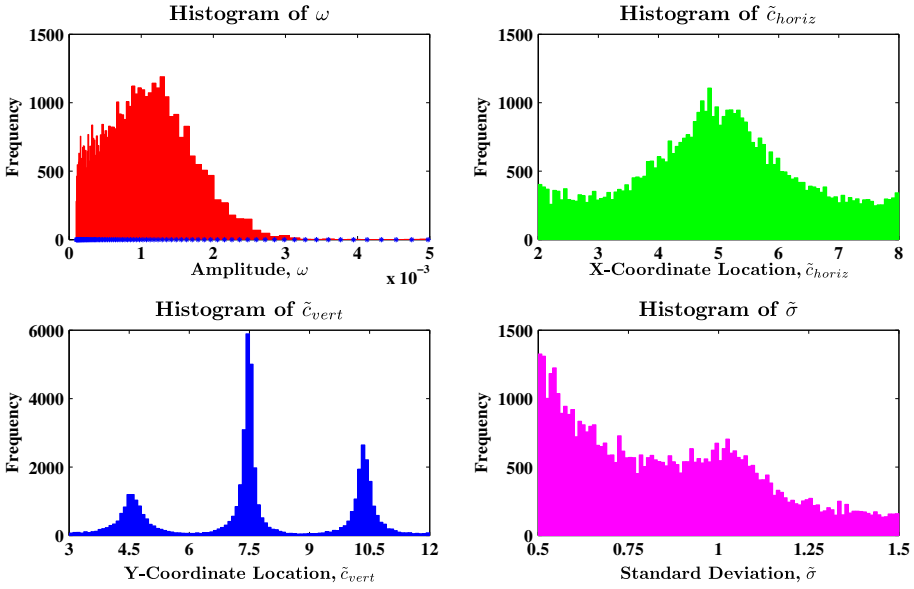

Fig. 9. One RBF: histograms of posterior parameters for noise-contaminated case (locations as in Fig. 5).

within a more intuitive three-dimensional context. Fig. 8 then provides an illustration of the absolute difference between the target imperfection field and the mean imperfection field resulting from the inference process. Of course, such a comparison assumes the mean imperfection field as an appropriate generalization of a multivariate stochastic process; at least with respect to the model parameters, $\tilde{c}$, this assumption appears reasonable.

Upon examination of the noise free data, it is noticed that the solution procedure yields a non-negligible noise variance estimate (*i.e.* consistent with an SNR on the order of 100.) This source of noise emanates from the differences in the meshes used to generate $\vec{u}^{exp}$ and $\vec{u}^{FEA}$ (*i.e.* ≈200,000 and ≈50,000 dofs, respectively). This result actually supports the claim made in [29]: that different mesh densities may sometimes be adopted as a means for introducing noise into an inverse solution process without explicitly injecting noise.

4.1.2. Noise-contaminated results

Moving now to the noise-contaminated case for the one RBF context, Fig. 9 provides scaled PDFs similar to those funrnished in Fig. 6. However, focusing attention on the *vertical* scales of these figures, it can be seen that the presence of noise does indeed have an impact on the solution uncertainty, as compared to the noise free case. For example, the peak frequency in the lower-left plot in Fig. 6 is 8000, whereas the analogous plots in Fig. 9 (*i.e.* the noise-contaminated case) display a peak frequency of 6000. Additionally, the amplitude factor, appearing in the upper-left of these same plots, displays a distribution that seems to "flatten", with the occurrence of additional noise. Translated, this gives evidence that: (1) the noise-contaminated data yield an amplitude parameter that is less certain; and (2) the vertical location parameter is more likely (albeit *slightly*) to err toward the lower and higher values, as noise increases.

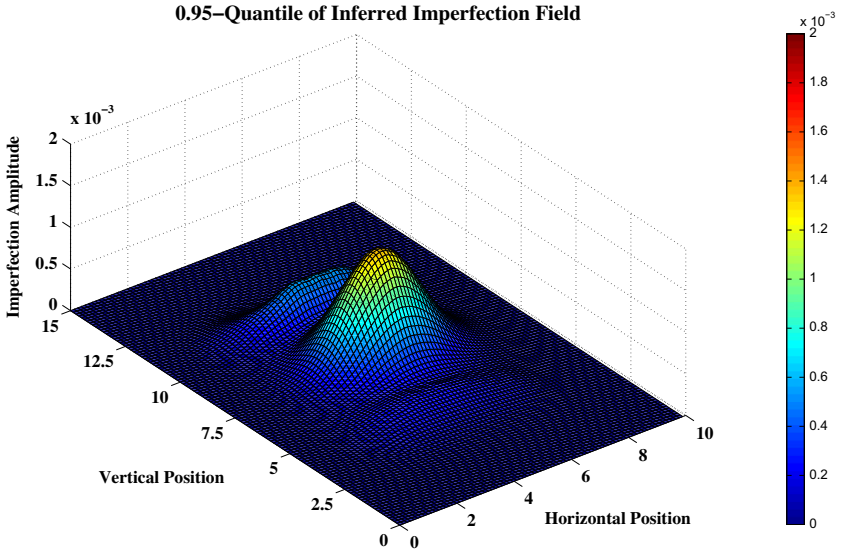

Fig. 10. One RBF: 95% Quantile of denting imperfection for noise-contaminated case (magnified ≈ 2700x).

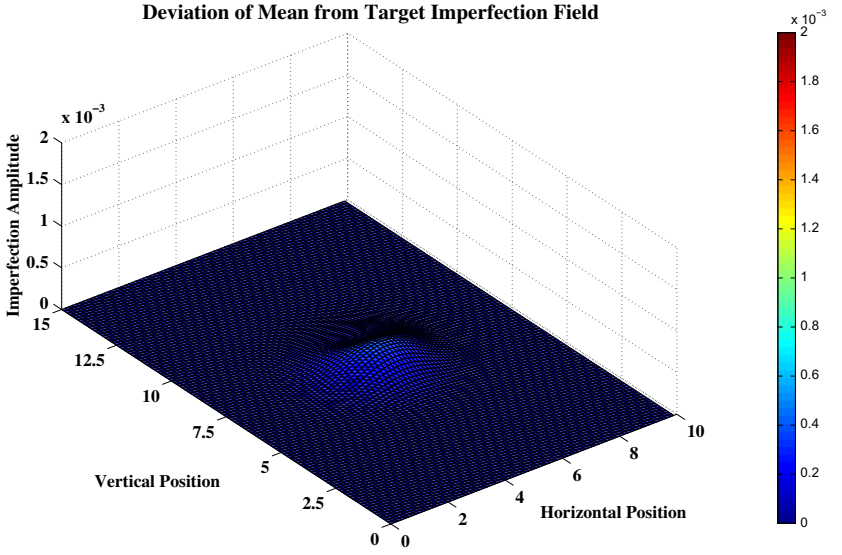

Fig. 11. One RBF: deviation of mean from the target imperfection field for noise-contaminated case (magnified ≈ 2700x).

The above statement, with regard to the amplitude parameter, is further confirmed by Fig. 10 where the imperfection amplitude, which captures 95% of the candidate solutions accepted by the MCMC algorithm, is less than that resulting from the noise free case (≈1.3 vs. ≈1.5, respectively.) Interestingly, however, the mean imperfection field for the noise-contaminated case, aligns more closely with the target imperfection field (see Fig. 11.) This is likely explained by the tendency of the amplitude parameter to assume a lower value, whereas in the noise free case, higher amplitudes (*e.g.* two or three times the target amplitude) are more prevalent.

As noted in the discussion on the noise free results, the primary source of noise in the modeling may be attributed to the projection error, arising from different finite element mesh densities employed is computing $\vec{u}^{exp}$ and $\vec{u}^{FEA}$, respectively. However, in spite of this fact, there are still measurable differences in the posterior parameter distributions arising as a result of the additional noise injection. This would imply that the the problem at hand is quite sensitive to noise, since differences in posterior parameter distributions are observed when increasing the SNR value by 1000 (from a baseline value of ≈100).

4.2. 4 RBF context

Recalling that, for brevity, the noise free case employing the four RBF imperfection context is being omitted, we next move forward to the noise-contaminated case. Examination of the chain behaviors given in Fig. 12 reveals significantly different results, as compared to the one RBF imperfection context. This behavior is somewhat expected, considering the inference process is driven by the *cumulative* effects of the four RBFs. As such, attention in this section is focused on the 95%-Quantile given in Fig. 13.

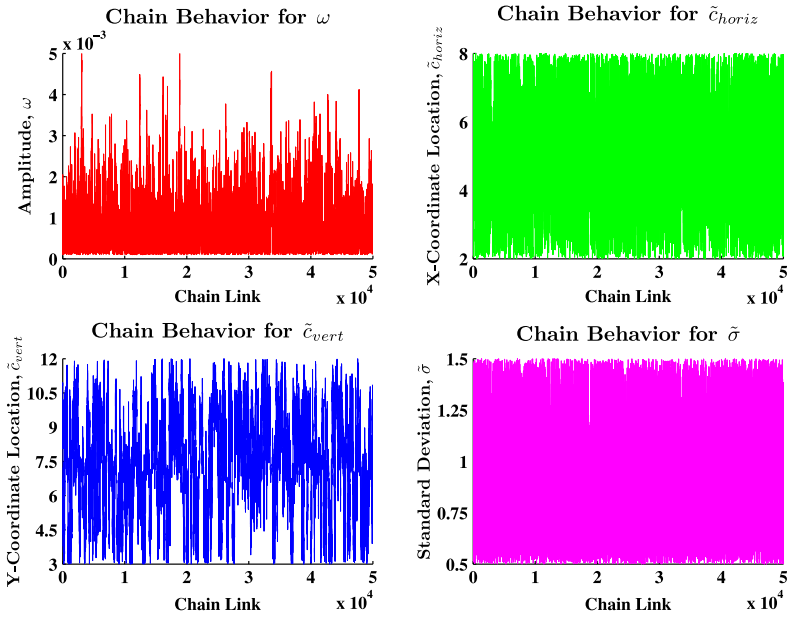

Fig. 12. Four RBF: representative Markov Chain behaviors in subset of posterior parameters for noise-contaminated case: upper-left - amplitude; upper-right - horizontal location; lower-left - vertical location; lower-right - standard deviation.

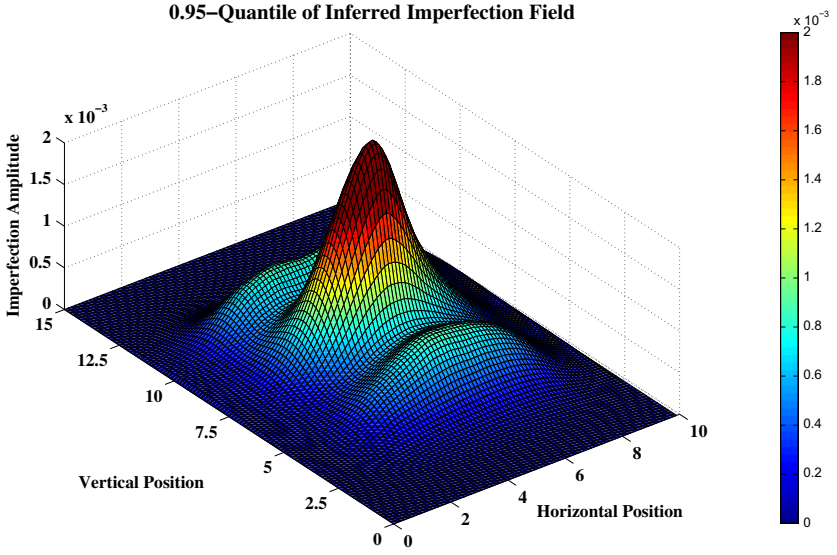

Fig. 13. Four RBF: 95% Quantile of denting imperfection for noise-contaminated case (magnified ≈ 2700x).

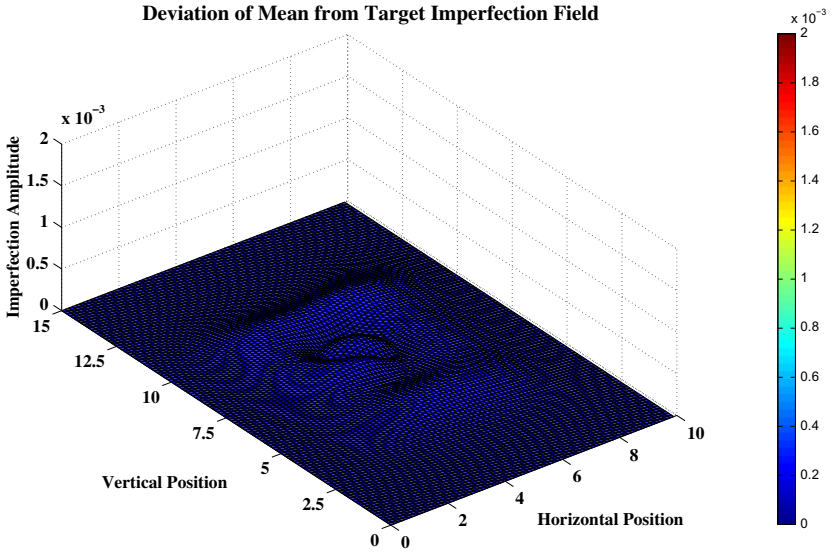

Fig. 14. Four RBF: deviation of mean from the target imperfection field for noise-contamined case (magnified ≈ 2700x).

As indicated by this figure, the four RBF imperfection context increases the plausibility of a greater range of posterior parameters, which define the solution space (*i.e.* previously less likely solutions are now more likely for this imperfection context.) A possible explanation of this result is that the allowable basis dimension, describing the imperfection field, is too large for the problem at hand. Attempting to infer the presence of a single denting imperfection, employing a four RBF imperfection context, may result in a sort of over-fitting problem in which the algorithm cannot resolve the addition of twelve model parameters, which could easily be characterized as non-essential, given the target. Of course, this *a priori* knowledge (*i.e.* knowing how many denting imperfections were present) would not be available in a typical application, and the need for such an imperfection model would be indispensable in cases where the nature of the imperfection field was unknown.

Consistent with the foregoing, the deviation of the mean imperfection field from the target imperfection field highlights that, for the four RBF context, the imperfection is more likely to be located above and below the target imperfection, than was seen in the one RBF context. Fig. 14 reveals that the deviations in this case are still reasonable.

5. Conclusions

Detecting the presence of, and quantifying the affects of geometric imperfections in shell structures represents an ongoing area of research, which encompasses myriad disciplines within the structural mechanics community. The present paper presents a unique contribution to this research topic, highlighting the importance of adopting a probabilistic approach to the characterization of geometric imperfections.

A methodology, formulated from the Bayesian interpretation of probability, has been presented which successfully characterizes, in probabilistic terms, a geometric imperfection field on a barrel vault type shell structure. In contrast to the oftentimes relied-upon MLE approaches, the results presented herein provide *quantifiable* evidence as to the plausibility of imperfection fields in the structure.

Continuing along this line of inquiry, the uncertainty associated with the inferred model parameters can now be propogated forward into the instability problem discussed in [29], allowing one to *probabilistically* characterize the buckling strength of the imperfect shell structure, rather than providing a point estimate of this quantity.

While the results presented herein are promising, it is not clear that the proposed method will yield similar results across all shell structures, and across all imperfection types. This current work is merely a point of departure, from which additional studies may be made.

Acknowledgments

The authors gratefully acknowledge the Office of Naval Research, Division 331, Ship System and Engineering Research, for their support of this work through Grants N00014–09-1–0532 and N00014–09-1–0310. The authors would also like to thank Dr. Paul Hess of Division 331 for his many helpful discussions.

References

[1] K.J. Bathe, E.N. Dvorkin, On the automatic solution of nonlinear finite element equations, Comput Struct 17 (5–6) (1983) 871–879.
[2] K.J. Bathe, E.N. Dvorkin, A four-node plate bending element based on mindlin/reissner plate theory and a mixed interpolation, Int J Numer Meth Engrg 21 (1985) 367–383.
[3] K.J. Bathe, E.N. Dvorkin, A formulation of general shell elements – the use of mixed interpolation of tensorial components, Int J Numer Meth Engrg 22 (1986) 697–722.
[4] Z.P. Bazant, L. Cedolin, Stability of structures, Oxford University Press, 1991.
[5] C.M. Bishop, Pattern recognition and machine learning, Springer, 2006.
[6] E.N. Dvorkin, K.J. Bathe, A continuum mechanics based four-node shell element for general nonlinear analysis, Engrg Comput 1 (1983) 77–88.
[7] B.L.O. Edlund, Buckling of metallic shells: buckling and postbuckling behaviour of isotropic shells, especially cylinders, Struct Control Health Monitor 14 (2007) 693–713.
[8] C.A. Featherston, Imperfection sensitivity of curved panels under combined compression and shear, Int J NonLinear Mech 38 (2003) 225–238.
[9] W.R. Gilks, S. Richardson, D.J. Spiegelhlater, Markov chain Monte Carlo in practice, Chapman and Hall, 1996.
[10] R.L. Hardy, Theory and applications of the multiquadratic-biharmonic method, Comput Math Appl 19 (8/9) (1990) 163–208.
[11] W.K. Hastings, Monte Carlo sampling methods using markov chains and their applications, Biometrica 57 (1) (1970) 97–109.
[12] J. Kaipio, E. Somersalo, Statistical and computational inverse problems, Springer, 2005.
[13] Kristanič, J. Korelc, Optimization method for the determination of the most unfavorable imperfection of structures, Comput Mech 42 (2008) 859–872.
[14] H.P. Langtangen, Computational partial differential equations, Springer, 2000.
[15] W.A. Link, R.J. Barker, Bayesian inference with ecological examples, Academic Press, San Diego, Ca, 2010.

[16] N. Metropolis, A.W. Rosenbluth, M.N. Rosenbluth, A.H. Teller, E. Teller, Equation of state calculations by fast computing machines, J Chem Phys 21 (6) (1953) 1087–1092.
[17] Neal RM. Probabilistic inference using markov chain Monte Carlo methods. Technical Report CRG-TR-93-1, Department of Computer Science, University of Toronto, Ontario, Canada, 1993.
[18] Neal RM. Suppressing random walks in markov chain Monte Carlo using ordered overrelaxation. Technical Report 9508, Department of Statistics, University of Toronto, Ontario, Canada, 1995.
[19] V. Papadopoulos, M. Papadrakakis, Finite-element analysis of cylindrical panels with random initial imperfections, J Engrg Mech 130 (8) (2004) 867–876.
[20] V. Papadopoulos, M. Papadrakakis, The effect of material and thickness variability on the buckling load of shells with random initial imperfections, Comput Meth Appl Mech Engrg 194 (2005) 1405–1426.
[21] V. Papadopoulos, I. Pavlos, The effect of non-uniformity of axial loading on the buckling behavior of shells with random imperfections, Int J Solids Struct 44 (2007) 6299–6317.
[22] V. Papadopoulos, G. Stefanou, M. Papadrakakis, Buckling analysis of imperfect shells with stochastic non-gaussian material and thickness properties, Int J Solids Struct 46 (2009) 2800–2808.
[23] B.D. Reddy, Introductory functional analysis, Springer, 1998.
[24] Rush, Show don't tell. Presto, Atlantic Records, 1989.
[25] D. Schillinger, V. Papadopoulos, M. Bischoff, M. Papadrakakis, Buckling analysis of imperfect i-section beam-columns with stochastic shell finite elements, Comput Mech 46 (2010) 495–510.
[26] J. Singer, J. Arbocz, T. Weller, Buckling experiments, Vol. 1, John Wiley and Sons, Inc., 1998.
[27] J. Singer, J. Arbocz, T. Weller, Buckling experiments, Vol. 2, John Wiley and Sons, Inc., 2002.
[28] J.C. Spall, Introduction to stochastic search and optimization: estimation, simulation and control, John Wiley and Sons, Inc., 2002.
[29] C.J. Stull, C.J. Earls, W. Aquino, A posteriori initial imperfection identification in shell buckling problems, Comput Meth Appl Mech Engrg 198 (2008) 260–268.
[30] A. Tarantola, Inverse problem theory and methods for model parameter estimation, Soc Ind Appl Math (2005).